npj | clean water

www.nature.com/npjcleanwater

ARTICLE OPEN

Check for updates

Ultrastable Co-NC membrane for sterilization of *Escherichia coli* in flowing water

Chao Li[1], Jiale Li[1], Niu Huang[1]✉, Xin Ying Kong[2], Qingyi Xiao[1], Yingping Huang[3], Po Keung Wong[4] and Liqun Ye[1,3]✉

Advanced oxidation technology based on peroxonosulfate (PMS) has attracted extensive attention in water treatment research due to its fast reaction speed and wide pH range adaptability. Cobalt-based catalysts are considered to be one of the most effective reagents for PMS activation in various PMS activation methods. However, Co-ion leaching and difficulty in recovery have greatly hindered its practical applications. Herein, we developed a robust membrane constructed by nitrogen-doped carbon nanotubes embedded with cobalt nanoparticles (Co-NC) to concurrently address the Co-ion leaching and recovery issues. Based on our customization, continuous water flow reactor, the Co-NC membrane exhibited excellent catalytic activity and stability, in which it demonstrated a remarkable sterilization efficiency of 99.9999% against *E. coli*, and it retained a superior stability of 96.29% after 40 repeated cycles. Fewer attempts to put such efficient heterogeneous advanced oxidation processes (AOPs) into practical application, to mimic real-life applications, the performance of the Co-NC/PMS system was extended to the water taken from Qiuxi River. Remarkably, there is no deterioration in performance over 12 h of continuous real sewage processing. Mechanistic studies revealed that abundant high-valence metals (Co^{IV}=O) were generated in the system, which can attack and penetrate into the cell membrane to destroy its intracellular defense system. This work provides useful insights into designing robust membranes with superior efficiency and stability for PMS-based advanced oxidation technology.

npj Clean Water (2023)6:47 ; https://doi.org/10.1038/s41545-023-00259-5

INTRODUCTION

The scarcity of freshwater resources is a major public health concern in many regions of the world[1]. Environmental degradation has led to widespread microbial contamination of surface water or regenerated water[2], not to mention the high adaptability and rapid reproduction of bacteria in water have caused serious adverse effects on our health[3]. To this, the incidence of waterborne diseases remains high, even in countries with high sanitation standards[4]. Despite the conventional disinfection techniques such as ultraviolet (UV) disinfection, ozone disinfection, and the use of chlorine-containing disinfectants have been widely employed for regenerated water treatment, there are still some drawbacks in the applications[5–8]. For instance, some biohazards are naturally resistant to UV light and chlorination[9]. In addition, disinfection by-products (DBPs) such as trihalomethanes[10], haloacetic acids formed by chlorination[11], as well as the toxicity and corrosiveness of ozone should not be neglected[12]. Therefore, there is an urgent need to develop a new, highly efficient, and harmless disinfection technology to reduce microbial colonies that might be harmful to public health.

In recent years, advanced oxidation processes (AOPs) are known to be more efficient than traditional water disinfection processes in inactivating biohazards due to its more efficient inactivation capability and lower tendency to form DBPs[13–16]. Compared to the traditional hydrogen peroxide-AOPs, persulfate-AOPs are more stable and the reagents are easier to store[17]. Specifically, thanks to its asymmetric structure and relatively longer O–O bond length, peroxymonosulfate (PMS) can be activated more easily by a myriad of catalysts[18,19]. Furthermore, PMS can be activated over a wide pH range (pH = 2.0–10.0) via multiple pathways to produce active species via either free radical or non-free radical pathways (e.g., $SO_4^{\bullet-}$ $E^o = 2.5–3.1$ V and half-life of 30–40 μs; $^{\bullet}OH$ with $E^o = 1.8–2.7$ V and half-life of 20 ns; $^1O_2$ with $E^o = 2.2$ V and half-life of 2 μs)[20–22].

Recently, transition-metal-ion redox couples have been directly used for activating PMS without needing external energy inputs[23–25]. Among them, the utilization of cobalt ion-based catalysts in AOPs has received far more attention[26–28]. Nonetheless, the difficulty in recovery and leaching of cobalt, which is a potential carcinogen have enormously impeded its practical applications[29]. Thereby, instead of using soluble cobalt in homogeneous catalytic systems, recoverable heterogeneous cobalt-based catalysts have been developed and adopted to activate PMS to reduce metal leaching[23]. Although the ion-leakage issue can be lessened to a certain degree, heterogeneous slurry systems often involve cumbersome and expensive catalyst recovery steps, including magnetic separation, precipitation, centrifugation, filtration, etc. Moreover, most of the existing catalysts for AOPs systems possess limited stability and lack of scalability, which curtail the practical application of this technology.

Recently, carbonaceous materials have been extensively studied for the activation of heterogeneous PMS owing to their unique potential and environmentally friendly properties[10,12]. Notably, it has been reported that the combination of metal and carbon can effectively prevent the leakage of metal ions[30,31]. However, the intrinsic inertness of pristine carbon planes greatly limits its activation performance in PMS. To address this, doping with nitrogen is posed to promote the catalytic activities of carbons. As reported in the literature[32], cobalt immobilized on porous

[1]College of Materials and Chemical Engineering, Key Laboratory of Inorganic Nonmetallic Crystalline and Energy Conversion Materials, China Three Gorges University, Yichang 443002, China. [2]Division of Chemistry and Biological Chemistry, School of Physical and Mathematical Sciences, Nanyang Technological University, 21 Nanyang Link, Singapore 637371, Singapore. [3]Engineering Research Center of Eco-environment in Three Gorges Reservoir Region, Ministry of Education, China Three Gorges University, Yichang 443002, China. [4]School of Life Sciences, The Chinese University of Hong Kong, Shatin, Hong Kong SAR, China. ✉email: huangliu.ysxf@163.com; lqye@ctgu.edu.cn

nitrogen-doped graphene demonstrated remarkable catalytic activity in PMS-AOPs. Therefore, the combination of nitrogen-doped carbon and metal has been vigorously developed in terms of catalytic oxidation very recently.

Till date, the PMS-AOPs typically operate in discontinuous intermittent systems accompanied by poor scalability. Compared to the widely used powder dispersions at room temperature, it is limited by slow interfacial mass transfer for practical water treatment[33]. To address the above-mentioned issues, we successfully prepared metallic cobalt coated with nitrogen-doped carbon nanotubes (Co-NC) membranes and assembled them in a customized flow reactor system with broad scalability (easy for recycling and facile membrane replacement) to evaluate their performance for bacterial advanced oxidation. The experimental findings revealed that the developed Co-NC membrane exhibited superior catalytic activity and long-term stability for bacterial activation. More importantly, its application can be extended to river water and lake water, demonstrating its potential practical application for complex water environments. The work is of paramount significance for the development of a highly efficient water treatment system with great potential for large-scale applications.

RESULTS AND DISCUSSION

Preparation and characterization of Co-NC membranes

Co-NC membranes which are made up of metallic cobalt nanoparticles coated with nitrogen-doped carbon nanotubes, were prepared via a facile CVD approach, as illustrated in Fig. 1a. For comparison, other kind of membranes (comprised of metallic cobalt mixed with nitrogen-doped carbons, labeled as Co+NC) were prepared under identical synthetic conditions except in the absence of dicyanamide (DCA) and without the acid-corrosion step. Figure 1b shows the X-ray diffraction (XRD) patterns of Co-NC, Co+NC, and NC catalysts. Co-NC and Co+NC both comprise of cubic Co metal (PDF#15-0856) and graphitic carbon (PDF#41-1487). Of note, the Co metal phase in Co-NC exhibits a lower degree of crystallization than that of Co+NC; in contrast, carbon in Co-NC possesses a higher graphitization degree. The differences are caused by the DCA, in which its incorporation and pyrolysis can promote the dispersion of Co species, thus resulting in smaller Co-nanoparticle (NP) size and simultaneously facilitating the growth of graphitic carbon layers, and the amount of Co in Co-NC is less than Co+NC (Supplementary Table 1). Figure 1c and Supplementary Fig. 1 demonstrate the scanning electron microscopic (SEM) image of Co-NC, which is composed of nanotubes strongly twinned on the carbon fibers of a piece of carbon cloth substrate to form a robust membrane. The carbon fiber spacing is between 10 and 50 μm. Meanwhile, the morphologies of NC and Co+NC are displayed in Supplementary Fig. 2, respectively. Supplementary Fig. 3 shows the transmission electron microscope (TEM) image of Co-NC with a cowpea-like structure, wherein Co NPs are encapsulated in carbon nanotubes with sizes between 30–100 nm. Figure 1e illustrates the high-resolution transmission electron microscopy (HRTEM) image of Co-NC from the region marked by the red circle in Fig. 1d. As revealed, the Co NP is encapsulated by carbon layers, displaying a lattice spacing of 0.33 nm which belongs to the (002) crystal planes of 2H graphite. The selected area electron diffraction (SAED) of Co NP in Fig. 1e is displayed in Fig. 1f, in which the bright spots correspond to the (022), (113), and (111) crystal planes of cubic Co metal. The elemental mapping of Co-NC (Fig. 1g) indicates that the C, N, and O elements are uniformly distributed; meanwhile, Co atoms are located in the interior part. In addition, the homogenous distribution of N elements suggests that N atoms are successfully doped into carbon nanotubes. X-ray photoelectron spectroscopy (XPS) analysis was performed to reveal the surface composition of the catalysts. The XPS survey spectrum of Co-NC in Supplementary Fig. 4 further discloses that Co-NC comprises of the C, O, N, and Co elements. Based on the high-resolution C 1*s* XPS spectrum (Fig. 1h), Co-NC exhibits four characteristic peaks corresponding to C-C/C=C (284.8 eV), C-N (285.71 eV), C-O (287.53 eV), and C-C=O (291.19 eV). Figure 1i displays the high-resolution N 1*s* spectrum of Co-NC, which can be deconvoluted into five peaks, including pyridinic N (398.78 eV), Co-N (399.73 eV), pyrrolic N (401.23 eV), graphitic N (402.48 eV), and oxidized N (404.08 eV). Figure 1j shows its Co 2*p* spectrum, where the Co 2p3/2 peak could be well fitted by Co-Co (778.84 eV), Co-O (780.58 eV), Co-N (782.58 eV), and sat. phases (786.48 eV). Similarly, the corresponding Co 2*p*1/2 peak can be deconvolved into Co-Co (794.48 eV), Co-O (796.08 eV), Co-N (797.69 eV), and sat. phases (802.05 eV) as well. These material analyses adequately illustrate that Co NPs-encapsulated N-doped carbon nanotube (Co-NC) membranes are successfully fabricated. In addition, the Raman spectrum in Supplementary Fig. 5 reveals that the I_D/I_G ratio of Co-NC is 1.03 (greater than the standard of 1.00), indicating that there are abundant defect sites present in the sample. Moreover, the Co-NC membrane possesses decent hydrophilicity with a water contact angle of 23.5° (Supplementary Fig. 6). The pristine carbon cloth is somewhat hydrophobic (because the sp^2 carbon layer without defects is highly hydrophobic), while the N doping (which enhances the degree of defects in the carbon material) improves the hydrophilicity of the carbon nanotubes to some extent. The improved hydrophilicity also promotes mass migration at the catalyst/water interface, thus facilitating the operation of the mobile water treatment experiments.

Instrument design and feasibility analysis

To study the robustness, recoverability, and stability of our-developed Co-NC membranes, we have developed a homemade flow reactor for water treatment. Figure 2a–c show the setup for the flow reactor. The Co-NC membranes were tailored to a round shape with a diameter of *ca.* 2.3 cm and held in position by sealing rings (Fig. 2b). Membranes were arranged in series, and then connected to the tubings and a pump. More details on the assembly of the flow reaction device are provided in Supplementary Fig. 7. Firstly, the efficiency of nanotube encapsulation on Co NPs for inhibiting Co leaching was studied. The concentration of Co ion in the filtrate was measured by ICP, and the results are shown in Fig. 2d. For the Co-NC membrane, the Co ion concentrations in the filtrate are measured to be 13, 9, and ~0 μg L^{-1} (fall below ICP detection limit), corresponding to one, three, and six times of filtration, respectively. In contrast, when Co-NC membranes were replaced by Co+NC, severe Co leaching was observed, in which the concentration exceeded the environmental standard for surface water (GB3838-2002, i.e., 1 mg L^{-1}) or the limit set for reclaimed water (US EPA reclaimed water limit, i.e., 50 μg L^{-1}) even after six times of flow treatment.

To preliminarily evaluate the AOPs catalytic performance of the fabricated Co-NC membranes, red rhodamine B (RhB) was used as a probe for organic pollutant removal. As displayed in Fig. 2e, Supplementary Fig. 8, and Supplementary Video 1, flowing through the apparatus only once with a high flux of 362 L m^{-2} h^{-1} (flow rate of 10 mL min^{-1}, four membranes in series arrangement), the filtrate turned to colorless with the degradation efficiency of 100%. Subsequently, the long-term stability of the Co-NC/PMS system is evaluated. There are no changes to the Co-NC catalytic performance after a continuous flow reaction of 30 h. Furthermore, the degradation rate is held at ~93% (average) via adopting 723 L m^{-2} h^{-1} flux, and the rate could be nearly 85% even under flux high as 1448 L m^{-2} h^{-1} (Fig. 2f). Notably, the experiment as well suggested the Co-NC membranes are of robust, as there are no cracks, wrinkles, or color changes after such high flow rate and long-term reaction. Subsequently, *Escherichia coli* (*E. coli*) was

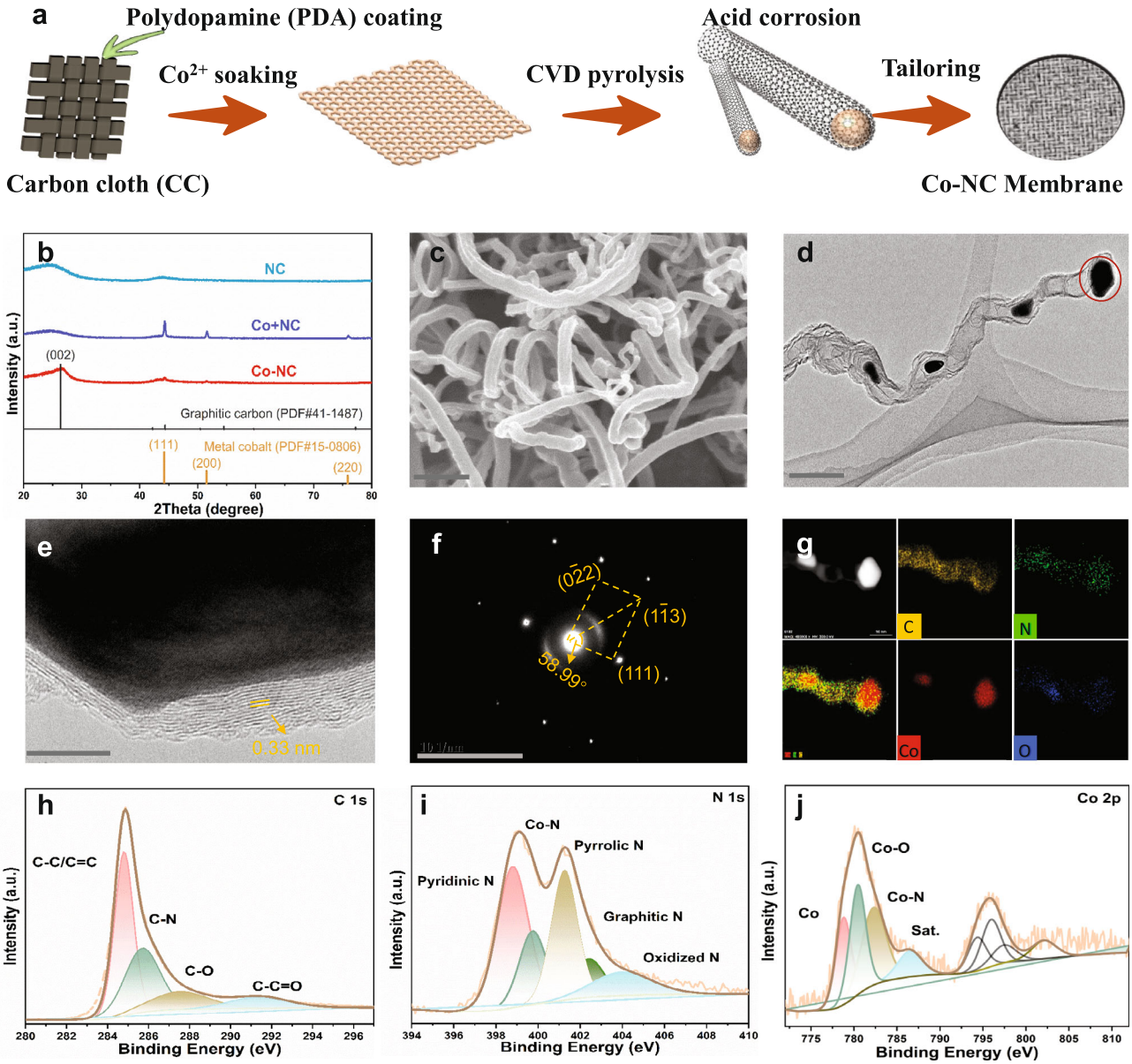

Fig. 1 Characterization of Co-NC membranes. a Schematic diagram for the synthesis of the Co-NC membrane. **b** XRD patterns of Co-NC and its counterparts. **c** SEM, **d** TEM, and **e** HRTEM images of Co-NC. The scale bars in Fig. 1c–f are of 1 μm, 200 nm, 10 nm, and 10 nm^{-1}, consecutively. **f** Selected area electron diffraction (SAED) of the Co nanoparticle in Fig. 1e. **g** Energy dispersive X-Ray spectroscopy (EDX) elemental mappings of C, N, Co, and O of Co-NC. **h** C 1*s*, **i** N 1*s*, and **j** Co 2*p* High-resolution XPS spectra of Co-NC.

chosen as a microorganism pollutant subject to test the efficiency of our-developed membranes. The sterilization ability of our fabricated Co-NC membrane-based flow reactor was measured and compared with other filters, including CC, filter paper, NC, and Co+NC, as shown in Fig. 2g and Supplementary Fig. 9. Filter paper and pure CC both exhibited weak sterilization capability (Fig. 2g insets), where the amount of *E-coli* was only decreased to $10^{6.5}$ cfu mL^{-1} and 10^{6} cfu mL^{-1}, respectively. The sterilization probably originated from physical flowing-and-filtering-caused damage to the cells. In contrast, the bactericidal effects over Co metal-contained catalysts (Co-NC and Co+NC) are fabulous, in which the bacteria were almost completely killed (>99.9999%) after six times of filtration. When adopting NC, the amount of *E-coli* was dropped to $10^{5.1}$ cfu mL^{-1} (Supplementary Fig. 9). While the sterilization effect is better than those of filter paper and pure CC, it is still much inferior compared to Co-NC and Co+NC. The results suggest that the PMS activation is dominantly led by metal sites (NC contributes a small part) to generate active species to kill *E-coli*. Notably, in the first cycle, Co+NC exhibited 100% sterilization efficiency, which is even more superior than Co-NC (Fig. 2h). This could probably caused by the Co leaching (Fig. 2d), which could activate PMS through homogeneous catalytic reactions to initiate AOPs to improve the sterilization. However, a high concentration of Co ions is tremendously hazardous. In addition, Co-NC membranes as well exhibited efficient inactivation activity against Gram-positive bacteria (*S. aureus*) with almost 100% sterilizing efficiency, as shown in Supplementary Fig. 10. Besides, the PMS activation performance of the Co+NC is not sustainable, as shown in Fig. 2h. Since the stability of catalyst for repeated usage is one of the critical factors to determine its suitability for practical applications, long-term stability tests for repeated usage were performed. The bactericidal performance of Co+NC membranes decreased to 41.66% after 40 repeated cycles (each cycle contains 6 times of filtration). On the contrary, Co-NC

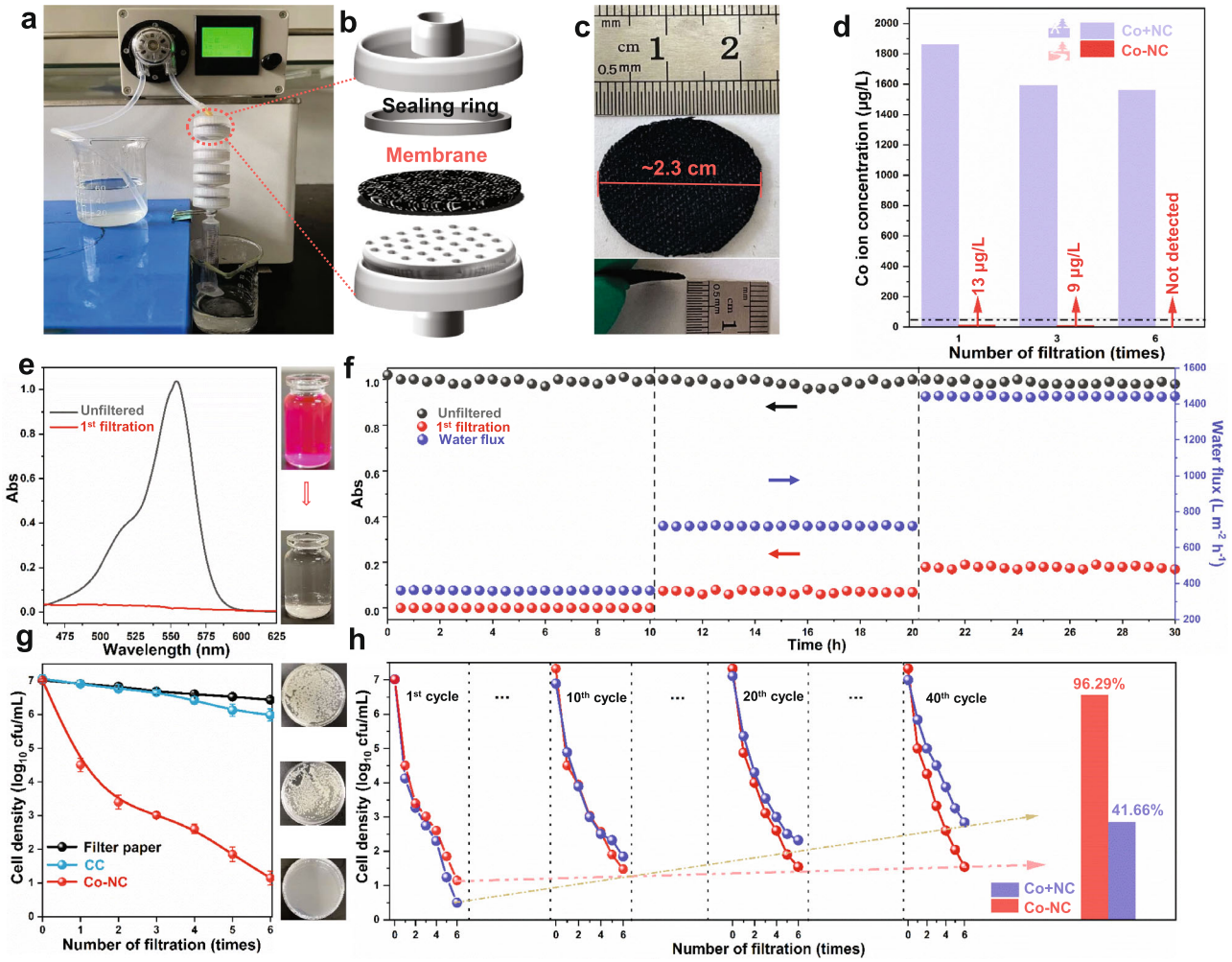

Fig. 2 Research on the performance of continuous flow device based on Co-NC membrane design. a Experimental setup for the flow reaction. **b** Schematic illustration for the assembly of a membrane in the system. **c** Dimensions of the membrane used in the experiment. **d** Concentration of Co ion in the filtrate after 1, 3, and 6 times of filtration using Co-NC and Co+NC membranes. **e** Absorption spectra of RhB solution before and after one time of filtration (insets show the color changes). **f** Absorption of RhB filtrate under 362, 723, and 1448 L m^{-2} h^{-1} flow rates, where each data point was taken at every half an hour interval for a total of 30 h for long-term evaluation. **g** Comparison of the sterilization efficiency over filter paper, pure CC, and Co-NC membrane, and their respective *E. coli* photographs after six times of flow reaction. **h** Sterilization performance and stability tests of Co-NC membrane and Co+NC membrane for repeated usage (up to 40 cycles). Experimental conditions: four Co-NC membranes connected in series (as shown in Fig. 1), water flux of 362 L m^{-2} h^{-1}, applied PMS concentration of 1.5 mM, bacterial solution (10^7 cfu mL^{-1}), and pH = 7.

membranes manifested excellent cycling performance, in which they retained a remarkable 96.29% of stability after 40 repeated cycles (240 times of filtration). Notably, the bacteria kill efficiency is around 99.9997% even after 40 repeated cycles (10^7–$10^{1.48}$/10^7).

Meanwhile, the bacterial solution is monitored after 40 cycles, it is found that the bacterial solution treated with the Co+NC membrane gradually became turbid while the Co-NC membrane reaction still remained transparent (Supplementary Fig. 11), which further demonstrated that the Co-NC mobile phase catalytic system exhibits excellent catalytic activity and stability. The morphology and structure of the membranes after the cycling test were further tested. The SEM images in Supplementary Fig. 12 show that the morphological structure of Co+NC thin film dramatically changed after 40 cycles. This could be attributed to its unstable structure and lack of acid resistance ($SO_4^{\bullet-} + H_2O \rightarrow {}^{\bullet}OH + H^+ + SO_4^{2-}$, $Co + 2H^+ \rightarrow Co^{2+}$). On the contrary, the morphology and structure of the Co-NC films remained unchanged (Fig. S12c, d). From XPS analyses (Supplementary Figs. 13, 14), the Co 2*p* spectra showed that the metallic Co was slightly oxidized after the cycling test, which led to slight changes to its catalytic activity. Nonetheless, the remarkable 96.29% stability (Fig. 2h) of the Co-NC were attributed to the stable coating of tubular nanotubes on Co NPs, suggesting that the Co-NC membrane is very promising for large-scale and long-term applications.

External factors influencing on Co-NC/PMS system

In order to investigate the practicability of the Co-NC membrane for water disinfection, different experimental conditions (including concentration, pH, flow rate, presence of inorganic anions, and humic acid (HA) concentration) of the Co-NC/PMS system were systematically studied. As shown in Fig. 3a, when the membranes were gradually added, the increase in the number of membrane layers corresponded to an increase in the catalyst concentration, which provided more active sites for PMS activation, resulting in forming more active species. When membrane layers were increased to 5, the deactivation rate was not significantly elevated. This indicates that the four layer Co-NC membrane can completely consume PMS, and the concentration of active species has reached the equilibrium point. Therefore, the following experiments were conducted using four layer Co-NC membranes. In

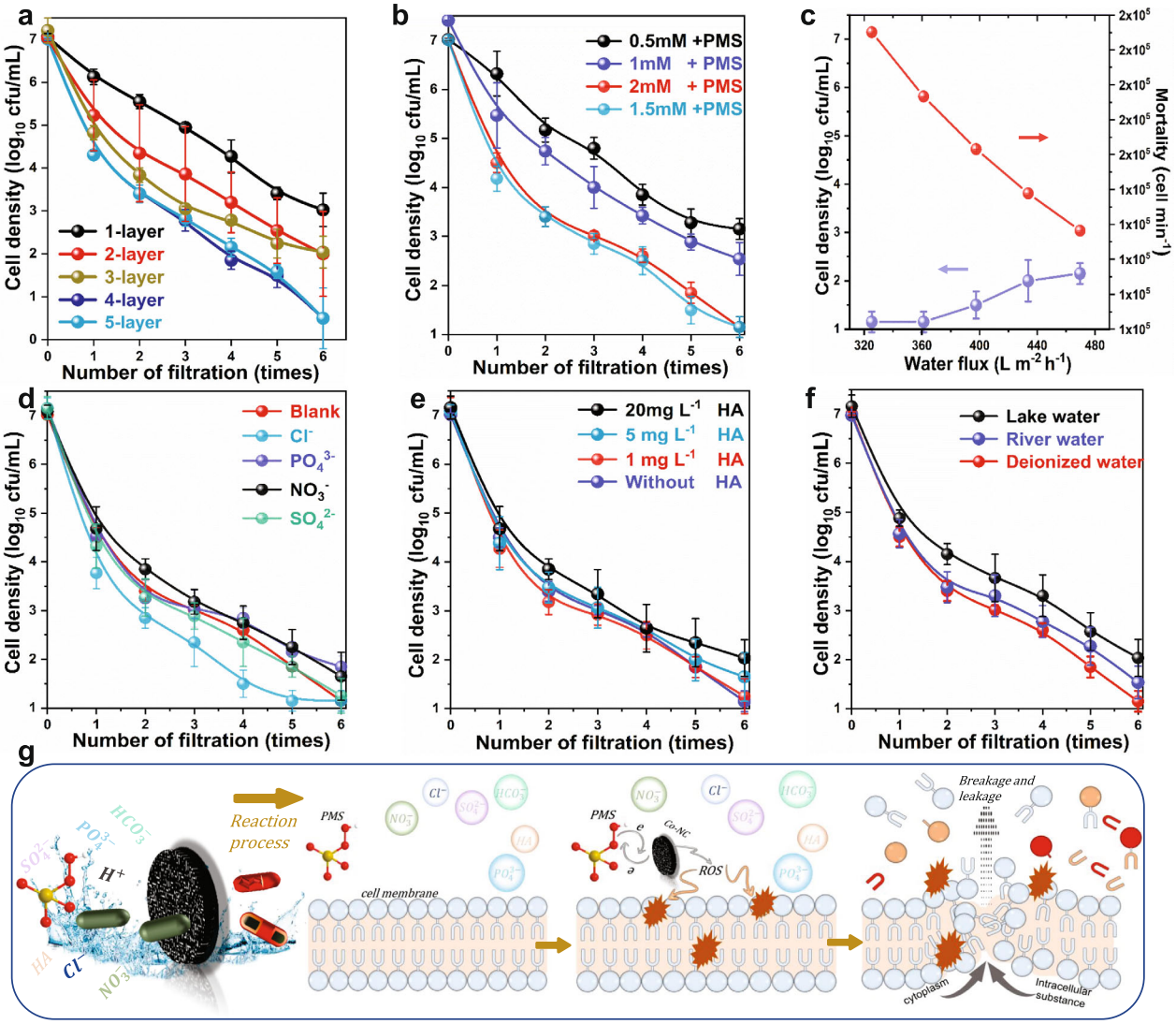

Fig. 3 Effects of different experimental conditions on the inactivation of bacteria by Co-NC membranes. a Membrane layers. **b** PMS dosage. **c** Water flux. **d** Presence of inorganic anions (20 mM). **e** HA concentration and. **f** Water source to study the effects of various environmental factors on the efficiency of Co-NC/PMS system. **g** Schematic diagram of the proposed mechanism for *E. coli* inactivation.

Fig. 3b, the inactivation rate of *E. coli* gradually increased (cell density reduced from ~10^3 to ~10^1 cfu mL^{-1}) with the increase in PMS concentration. Clearly, a reasonable increase in PMS concentration favors the generation of active speicies. However, the inactivation rate does not increase further with the PMS concentration when the concentration reaches 2 mM. Excessive PMS may result in the quenching of active species. Meanwhile, it is worth noting that the flow and efficiency in actual water treatment are always closely related to the flow rate in actual application. When the water flux increased from 325 to 469 L m^{-2} h^{-1} (Fig. 3c), the concentration ratio of the remained bacteria gradually increased from $10^{1.3}$ to $10^{2.0}$ cfu mL^{-1}, accompanied by a decrease in the inactivation rate (from 2×10^5 to 1×10^5 cells min^{-1}). This indicates that the high flow rate causes the cells to stay in the flow reactor for a short period of time, which restrains the effect of active species on the cells to a certain extent. Inorganic anions (NO_3^-, SO_4^{2-}, PO_4^{3-}, Cl^-, etc.) are widely present in various water bodies, which generally pose significant effects on the degradation of contaminants in conventional AOPs as the free radicals are usually scavenged by certain anions. As shown in Fig. 3d, it is noted that when NO_3^-, SO_4^{2-}, and PO_4^{3-} inorganic anions were added, the sterilization performance of *E. coli* did not be varied much. In addition, when Cl^- is present in the water column, it increases the inactivation energy of the Co-NC/PMS system. This may be due to the oxidation of Cl^- by partial •OH and $SO_4^{\bullet-}$ to produce chlorine radicals ($Cl^- + SO_4^{\bullet-} \longrightarrow Cl\bullet + SO_4^{2-}$, $Cl^- + \bullet OH \longrightarrow ClOH^{\bullet-}$, $Cl\bullet + Cl^- \longrightarrow Cl_2^{\bullet-}$), which also attack intracellular biomolecules and induce apoptosis. This provides the application possibility of the Co-NC membrane for inactivation in sea water[34,35]. On the contrary, when HCO_3^- exists in the water body (Supplementary Fig. 15), the sterilization performance was slightly deteriorated due to the interaction between PMS and HCO_3^{2-} to form peroxymonocarbonate to reduce PMS concentration. Additionally, the coordination of HCO_3- with Co(II) probably decreases the active sites of the system[36]. Ammonia usually presents in the wastewater; thus, its influence on AOPs catalytic performance was studied. As revealed in Supplementary Fig. 16, the addition of ammonia in the Co-NC/PMS system had little effect on the inactivation of *E. coli*. Figure 3e shows the effect of the concentration of HA on the disinfection performance. The increase of HA concentration in flow treatment did not cause significant changes to the disinfection performance. This observation manifests that the disinfection performance of the Co-NC/PMS

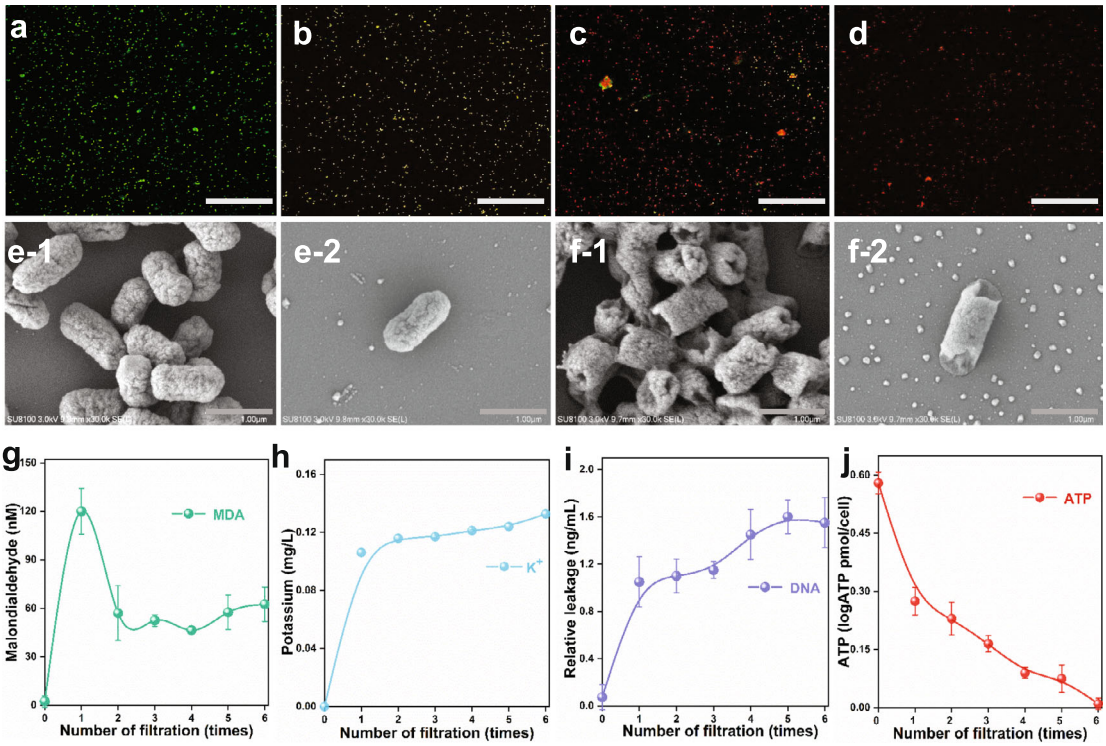

Fig. 4 Physicochemical characterization of *E. coli*. Fluorescence microscopy images of *E. coli* treated with our flow reactor consists of Co-NC membranes with filtration for **a** 0, **b** 1, **c** 3, and **d** 6 times. SEM images of *E. coli* **e** before and **f** after flow processing. The white and gray scale bars are of 100 and 1 μm, respectively. **g** Content of MDA. **h** The amount of K^+ leakage. **i** Leakage of DNA content in the solution. **j** ATP content in the cells.

system was not affected by the concentration of HA while keeping high efficiency. Figure 3f displays the disinfection performance of the Co-NC/PMS system in different river water and lake water samples to mimic real-life applications. In comparison with ultrapure water, the disinfection performance in river water and lake water was only slightly reduced. It indicates that regardless of the complexity of the water matrix, the flow system assembled by Co-NC membranes can still efficiently and safely disinfect the bacteria, even in real water samples. Under different environmental factors, the Co-NC/PMS system can still generate a large amount of active species to destroy the membrane phospholipids of *E. coli* and cause casualties (Fig. 3g). The above results demonstrate that the Co-NC membrane can be considered a promising technique for efficient inactivation of bacteria in real water samples.

Bacterial inactivation process

Fluorescence microscopy was used to detect the viability of *E. coli* by cell staining. Before the sterilization process, live cells exhibit strong green fluorescence (Fig. 4a). After the inactivation reaction using the flow reactor, as shown in Fig. 4b, green is transferred to yellow (caused by green and red fluorescent overlapping). With more rounds of filtration, more and more areas present red (Fig. 4c). Finally, green fluorescence was completely replaced by red fluorescence (Fig. 4d). It implies that the sterilization of *E. coli* involves the leakage of active substances in cells[37], which also evidenced by SEM images and leakage detection. As shown in Fig. 4e, the *E. coli* cell membrane was intact before treatment. However, after the flow treatment, all *E. coli* cells in the solution shrank, shattered, and twisted (Fig. 4f), indicating that *E. coli* cells were inactivated during the sterilization process. The results show that the *E. coli* cells were continuously destroyed under the flow treatment of the inactivation device until they were completely inactivated and died. On the other hand, the leakage of cell contents, membrane lipids, and adenosine triphosphate (ATP) were analyzed. Figure 4g shows that a large amount of malondialdehyde (MDA) was detected relative to the untreated bacterial fluid after different times of filtration, suggesting that the gradual oxidation of lipids leads to cell membrane damage. Figure 4h shows the gradual leakage of potassium ions, which increased from an initial 0 to 0.13 mg L^{-1}, which results in the release of cellular contents and respiratory depression. As the cell membrane is lysed and exuded, the bacterial genetic system is damaged, and the damaged cell envelope can also induce the release of cytoplasmic components (such as DNA), and the content of nucleic acids in the solution gradually increases (Fig. 4i). ATP is often referred as the energy currency in cells and it is the most direct source of energy in living organisms. As the bacterial solution gradually passed through the Co-NC membrane, the ATP content decreased from an initial 0.58 $\log_{10}$ATP pmol/cell to 0 after 6 times of filtration (Fig. 4j). It demonstrates that the energy metabolism system of the bacteria is damaged, and it cannot maintain the normal operation of various cellular functions.

Mechanism study

Reactive oxygen species have a strong oxidative capacity and are usually widely noticed for their important role in water treatment processes. To gain insight into the reactive species in the Co-NC/PMS system, several scavenging experiments were performed. As shown in Fig. 5a, without adding any capture reagent, the reaction rate constant of RhB degradation was 0.16 min^{-1}. When p-benzoquinone (PBQ) was added as the capture for $O_2^{\bullet-}$, the reaction rate was decreased merely to 0.142 min^{-1} (Fig. 5a), and the RhB degradation efficiency was slightly reduced from 100 to 96.1% (i.e., the inhibition rate is 3.9%, in Supplementary Fig. 17). Additionally, the produced amount of $O_2^{\bullet-}$ was quantified by using p-nitro-blue tetrazolium chloride (NBT). As revealed in Supplementary Fig. 18a,

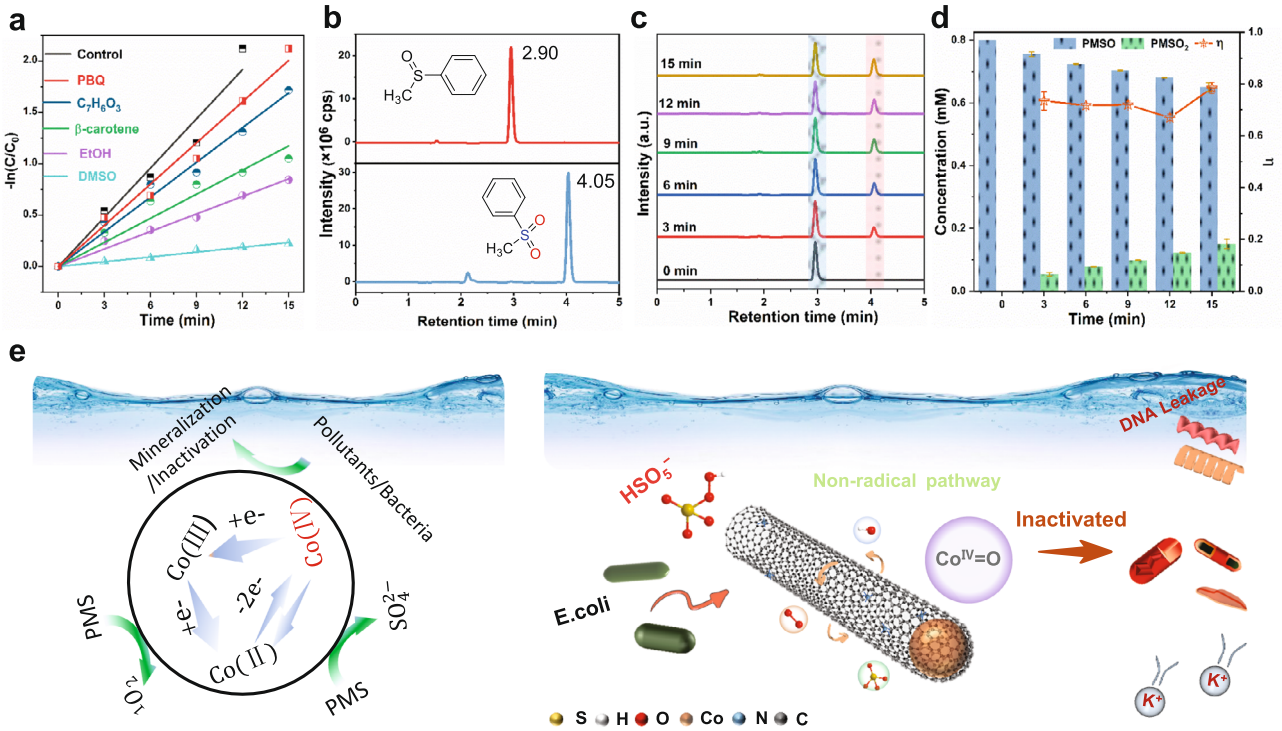

Fig. 5 Study on activation path and mechanism of Co-NC/PMS. a Kinetic curves in Co-NC/PMS system without/with adding different scavengers. **b** HPLC chromatograms of standard PMSO and $PMSO_2$. **c** HPLC chromatogram of PMSO consumption and $PMSO_2$ generation in the Co-NC/PMS system. **d** $\eta(PMSO_2)$ when adding PMSO into the Co-NC/PMS system. **e** Proposed mechanism of PMS activation and inactivation of *E-coli* in Co-NC/PMS system. [PMS] = 1 mM, Area of Co-NC membrane = 0.5 × 0.5 cm^2, [PBQ] = [$C_7H_6O_3$] = [β-carotene] = 20 mM, [EtOH] = 300 mM, [DMSO] = 2 mM, [PMSO] = 0.8 mM.

the absorbance of NBT at 259 nm was almost unchanged after 15 min (suggesting the amount of $O_2^{\bullet-}$ was scarce to cause the reduction of NBT) and the concentration of $O_2^{\bullet-}$ is estimated to be 8.2 μM at 15 min (Supplementary Fig. 18b). These results together indicate $O_2^{\bullet-}$ plays a faint (or negligible) role in the Co-NC/PMS system for pollution degradation. Supplementary Fig. 19 exhibits the ESR experiment results by using 5,5-dimethyl-1-pyrrolidine-*N*-oxide (DMPO) and 2,2,6,6 tetramethyl proline (TEMP) as spin traps, where the relatively strong signal peaks demonstrate the presence of $^{\bullet}OH$, $SO_4^{\bullet-}$, and $^1O_2$ (respectively forming as DMPO-$^{\bullet}OH$, DMPO-$SO_4^{\bullet-}$, and TEMP-$^1O_2$) in the Co-NC/PMS system. When salicylic acid was added as the capture for $^{\bullet}OH$, the reaction rate was decreased (Fig. 5a) with an inhibition rate of 14.5% (Supplementary Fig. 17). Simultaneously, $^{\bullet}OH$ concentration in the Co-NC/PMS system was determined by fluorescence luminescence spectroscopy, where benzoic acid (BA) was used as a probe to capture ●OH to form as hydroxybenzoic acid (HBA) with an emission peak at around 415 nm. Similarly, the produced ●OH concentration was evaluated to be about 0.86 μM at 15 min (Supplementary Fig. 20). These results together indicate ●OH plays a minor role in the Co-NC/PMS system for pollution degradation. Subsequently, ethanol with a high concentration of 300 mM was introduced to the Co-NC/PMS system, where ethanol can capture $SO_4^{\bullet-}$ and $^{\bullet}OH$ bursts with high reaction rates ($K_{SO4\bullet-/EtOH} = 10^7\ M^{-1}{\cdot}s^{-1}$, $K_{\bullet OH/EtOH} = 10^9\ M^{-1}{\cdot}s^{-1}$). It can be seen that the inhibition rate was increased to 42% (Supplementary Fig. 17). Similarly, the $SO_4^{\bullet-}$ concentration was evaluated via high-performance liquid chromatography (HPLC, Supplementary Fig. 21), and the $SO_4^{\bullet-}$ concentration produced at 15 min was about 42 μM. Notably, the adoption of ethanol probably triggers other effects, such as adsorption on the catalyst surface to reduce (even poison) the active sites or hinder electron transfer. Thus, the performance decline here (42%) probably were not only caused by $SO_4^{\bullet-}$ and $^{\bullet}OH$. Nevertheless, these results together disclose that $SO_4^{\bullet-}$ plays a certain role in the Co-NC/PMS system for pollution degradation. After that, β-carotene was used for inhibiting $^1O_2$, as shown in Fig. 5a and Supplementary Fig. 17, the carotenoid inhibition effect was about 29%, and the reaction rate constant was dropped to 0.078 min^{-1}. Similarly, the $^1O_2$ concentration was evaluated by using furfuryl alcohol (e) as scavenging for $^1O_2$ ($K_{FFA/^1O_2} = 1.2 \times 10^8\ M^{-1}{\cdot}s^{-1}$), and its concentration is estimated to be about 28.2 μM (Supplementary Fig. 22). These results together disclose that $^1O_2$ plays a certain role for pollution degradation. In a nutshell, the conventional active oxygen species, including radical and non-radical, are not the dominant active species in the Co-NC/PMS system. Among them, $^1O_2$ and $SO_4^{\bullet-}$ with relatively higher concentrations play certain roles in pollution degradation. Therefore, there are/is other activating agents/agent as the chief active species/specie. Dimethyl sulfoxide (DMSO) was introduced as an effective scavenger for high-valence metals[38], and DMSO could almost completely inhibit the degradation of contaminants at low concentrations (e.g., 2 mM). When DMSO was added to the Co-NC/PMS system, the RhB degradation rate constant was decreased to 0.015 min^{-1} (Fig. 5a) with an inhibition rate of about 85% (Supplementary Fig. 17) at 15 min. The preliminary result suggests that high-valence Co is the main active specie. Furthermore, methyl phenyl sulfoxide (PMSO) was introduced to the Co-NC/PMS system to react with the possible high-valence Co[39]. The standard PMSO and $PMSO_2$ spectra were examined (Fig. 5b and Supplementary Fig. 23), where the peak emerged at 2.90 min belongs to PMSO and the peak appeared at 4.05 min comes from $PMSO_2$ (their molecule structure are inserted in Fig. 5b)[40]. When PMSO is added to the Co-NC/PMS system, the intensity of PMSO is gradually decreased and the intensity of $PMSO_2$ is gradually increased, as revealed in Fig. 5c.

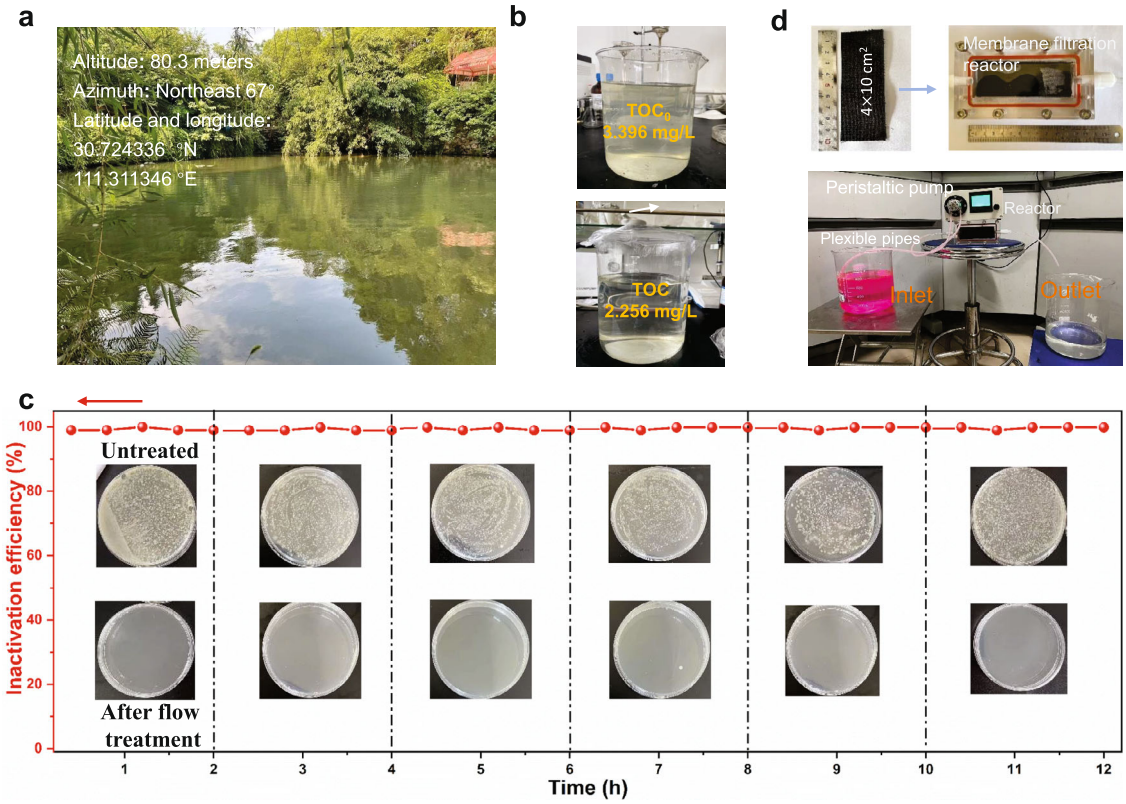

Fig. 6 Feasibility study on flow device composed of Co-NC membranes. a The location of Qiuxi River, photographs of water bodies, **b** TOC of water samples before and after treatment. **c** 12-h continuous flow treatment of Qiuxi River (The initial bacterial concentration in the wastewater is about 3–4 $\log_{10}$ cfu mL^{-1}. **d** Co-NC membrane connected filtration unit treatment photos, size of membrane = 4× 10 cm^2.

PMSO can be consumed by various pathways: oxidation by oxidizing agents, high-valence metals, and single electron transfer (forming as hydroxylated PMSO)[41]. As for $PMSO_2$, it can be produced by Co^{IV}=O and PMS in the Co-NC/PMS system. When only PMS was introduced to react with PMSO (without Co-NC membrane), the concentrations of PMSO and the generated $PMSO_2$ was detected (Supplementary Fig. 24). When PMSO was added to the Co-NC/PMS system, the concentrations of PMSO and the generated $PMSO_2$ was detected (Fig. 5d). As revealed, after 15 min, the produced amount of $PMSO_2$ was 0.139 and 0.037 mmol corresponding to the situations with and without Co-NC membrane, respectively. After deducting the produced amount of $PMSO_2$ by PMS, the yield rate of $PMSO_2$ by Co^{IV}=O ($\eta(Co^{IV}=O)$) was calculated and displayed in Fig. 5d. As revealed, the η kept above 72% during the whole oxidation process. These results clearly indicate that the high-valence metal (Co^{IV}=O) is the main active species in the Co-NC/PMS system.

Based on the above experimental results, the mechanism of the Co-NC/PMS system is shown in Fig. 5e. Through a two-electron oxidative transfer pathway, Co-NC is oxidized to form high-valence Co metal (Co^{IV}=O) as the primary active species (Supplementary Table 2, Equation 7). Through a single electron transfer pathway, $SO_4^{\bullet-}$ and $^1O_2$ were produced as secondary species (Equations 1, 3, and 6). Among them, $^1O_2$ is mainly derived from the nitrogen in Co-NC. The nitrogen exists in the form of graphitic N, pyridinic N, pyrrolic N, etc., which are highly selective to generate $^1O_2$ in the PMS-AOPs system[42,43]. According to the XRD pattern and TEM-EDS mapping images, most of the Co elements in the Co-NC are formed as Co metal nanoparticles, which means the high-valence metal state (Co^{IV}=O) is mainly originated from the surface oxidized Co metal nanoparticles (Co-O bonding, as shown in Fig. 1j, where Co-N comes from the interface bonding between Co metal and NC). Besides, the smaller electrical impedance also provides the favorable condition of the Co-NC membrane in terms of electron transport (Supplementary Fig. 25). In the case of *E. coli* (and *S. aureus*) inactivation, during water flow, the Co-NC membrane is used as the catalytic platform for the reaction between PMS and bacteria, where (on the Co-NC membrane surface) abundant Co^{IV}=O is generated, which will first attack cell wall/membrane and cause lipid peroxidation, leading to the damage of cell membrane. Then, other active species (such as $SO_4^{\bullet-}$, $^1O_2$, and $^{\bullet}OH$) cross the membrane and disrupt the intracellular defense system of cells, and subsequently, large amounts of potassium ions are leached out, further contributing to cell lysis. Cellular respiration is also interrupted and energy supply is gradually lost, which in turn affects cell viability, leading to the loss of key cellular functions (nucleic acids) and complete cellular inactivation eventually.

Analysis of extensibility and universality of the actual water body

In view of the excellent catalytic cycling performance of our-developed Co-NC/PMS system, this study was extended to practical applications by studying the real water sample from Qiuxi River (Fig. 6a). Subsequently, water samples were taken for the flow treatment as shown in Fig. 6b. Before treatment, the solution is turbid with TOC at 3.396 mg L^{-1}, which signifies that the water contains excess amounts of soluble organic matter. Besides, the real water sample has complex bacterial species (Supplementary Fig. 26) and high concentration of anions (Supplementary Table 3). After undergoing flow treatment by our-developed Co-NC/PMS system, the contaminated river water becomes much clearer with a decreased TOC of 2.256 mg L^{-1}. It

implies that the organic pollutants are effectively decomposed. More importantly, the Co-NC/PMS system can effectively disinfect live bacteria in real water with a remarkable and sustainable efficiency of 99.99% (Fig. 6c), even working continuously for 12 h. Notably, a large-size Co-NC membrane with $4 \times 10\ cm^2$ was also used to confirm the efficient treatment of contaminants by assembling another flow reactor (Fig. 6d, Supplementary Fig. 27, and Supplementary Video 2). The results as well demonstrate that the Co-NC/PMS system is sustainable for amplification to remove organic pollutants and inactivation of pathogenic microorganisms in water, which displays great application value in the field of water treatment.

In summary. Co-NC films are successfully fabricated for the inactivation of pathogenic microorganisms based on PMS advanced oxidation technology. It may be important for the rational design and metal precipitation of metal materials (including carbide and nitride, etc.). We also established a continuous flow system that can effectively degrade organic pollutants and inactivate bacteria. During water flow treatment, vast quantities of bacteria and pollutants are briefly "stagnated" through the membrane, which rapidly inactivates bacteria and degrades pollutants by generating a large amount of active species (high valent metals dominant), and then discharges. The system has good long-term performance and cycling stability, even in the actual complex water environment has shown good treatment performance and environmental tolerance. In the stability test, the catalytic activity maintained a remarkable efficiency of 96.29% after 40 test cycles, indicating the potential of the flow reaction system for large-scale catalytic applications. The system provides insight into the mechanism of action of the high-valence cobalt-oxygen products. In conclusion, our work provides a viable alternative to advanced oxidation technologies for efficient water disinfection, with a high potential for large-scale applications in industry.

METHODS

Materials

All reagents, including peroxymonosulfate (PMS, $0.5KHSO_4{\cdot}0.5K_2SO_4{\cdot}KHSO_5$) and ethanol (EtOH), are of analytical purity. LB Broth and Agar medium were supplied by Guangdong Huankai Microbial Sci. & Tech. Co., Ltd. Rhodamine B (RhB) was purchased from Sinopharm Chemical Reagent Co., Ltd. Dimethyl sulfoxide (DMSO), methyl phenyl sulfoxide (PMSO), methyl phenyl sulfone ($PMSO_2$), terephthalic acid (TA), p-nitro-blue tetrazolium chloride (NBT), p-hydroxybenzoic acid (HBA), and benzoquinone (BQ) were acquired from Aladdin Chemistry Co., China. Deionized (DI) water with a resistivity of 18.25 MΩ·cm was used in the experiment where specified. Carbon cloth (HCP330N) with a thickness of 0.29 ± 0.02 mm was purchased from Shanghai Hesen Electric Co., Ltd. Filter paper was purchased from Tianjin Jinteng Experimental Equipment Co., Ltd. The Yangtze River water sample was taken from the 1 km upstream of the Three Gorges Dam. The lake water samples were taken from Dongyuan Lake in China Three Gorges University and Qiuxi River (30.724336 °N and 111.311346 °E) in Yichang City, Hubei province of China. The pH and conductivity of Qiuxi River water, as well as the inorganic ions contained in the water sample, were measured and listed in Supplementary Table 3.

Synthesis of Co-NC and Co + NC

Firstly, polydopamine (PDA) nanolayer was homogeneously grown on carbon fibers of carbon cloth (CC) pieces (CC with the size of 2.5 cm × 5.0 cm). Secondly, these substrates were immersed in 800 mM $CoCl_2$ aqueous solution for half an hour to allow adequate adsorption of Co^{2+} ions on PDA. Thirdly, Co-NC membranes were prepared by a chemical vapor deposition (CVD) approach, where dicyanamide (DCA) served as a solid source placed upstream of a tubular furnace while the CC/ PDA-Co^{2+} pieces were placed in the middle of the furnace. The CVD pyrolysis was performed at 850 °C for 2 h under Ar flow. Ultimately, these membranes underwent acid corrosion (in 0.5 M H_2SO_4, at 80 °C for 24 h) to remove the Co nanoparticles unsheathed by graphitic carbon walls (i.e., those exposed outside carbon nanotubes). Co+NC membranes were prepared without introducing DCA in the CVD pyrolysis and without the last acid-corrosion step, otherwise identical synthetic conditions.

Flowing water disinfection process

The inactivation test was performed in a homemade flow reactor consisting of replaceable membrane elements, serpentine liquid channels, and a peristaltic pump. *E. coli* were cultured in LB broth for 16 h in a shaking incubator. Then, the bacterial solution was centrifuged at 10,000 rpm for 1 min with 0.85% saline and washed twice prior to use. About 1.5 mM PMS was added to the previously prepared sterilized water, then 25 mM H_2SO_4 and/or 25 mM NaOH were added dropwise to adjust the solution pH to 7. Subsequently, a 6 mL bacterial solution was added to the beaker containing 100 mL of sterilized distilled water, where the bacterial concentration in the system was about 10^7 cfu mL^{-1}. After taking the initial reading, the peristaltic pump was turned on for filtration, and the device took 100 μL of the reaction solution for each cycle of filtration. The obtained sample was diluted to an appropriate concentration, and then 100 μL of the diluted solution was added to an agar plate. Lastly, the agar plates were incubated in biochemical jars at 37 °C for 12 h.

Contaminant test: Rhodamine B (RhB) solution (10 mg L^{-1}) was firstly prepared, then added to 1.5 mM PMS and stirred to form a homogeneous solution. The peristaltic pump was then turned on for filtration. After each filtration cycle, 3 mL of the reaction solution was added to 1 mL of sodium thiosulfate (0.1 M) to quench free radicals for the termination of the reaction. After centrifugation at 8000 rpm, the supernatant was collected and analyzed by UV-Vis spectrophotometer (UV2600, Timemi) to detect the absorbance at 554 nm.

Fixed amounts of PMS and Co-NC membranes (0.5 cm × 0.5 cm) were added to a 50 mL beaker. With the addition of different reagents for different reactions, when experiments were carried out to complete, 1 mL of the reaction solution was extracted using a syringe and immediately mixed with an excess of Na_2SO_3 to quench the reaction products. The samples were then filtered through a hydrophobic membrane (0.22 μm) and the concentrations of organic compounds were further analyzed by high-performance liquid chromatography (HPLC) with a PDA detector (Waters 2690 chromatograph) equipped with a C18 column (4.6 × 250 mm, 5 μm particle size). To evaluate the amounts of furfuryl alcohol, the measurement conditions are as follows: mobile phase with a flow rate of 1 mL min^{-1}, 70/30% (v/v) mixture of methanol/water, and $\lambda = 230$ nm. To evaluate the concentration of benzoquinone, PMSO, and $PMSO_2$, the measurement conditions are as follows: 40/60%, 50/50%, and 50/50% mixture of acetonitrile/water, respectively, $\lambda = 215$ nm, and a flow rate of 1 mL min^{-1}.

Quantification of free radical concentration

To determine the concentration of •OH, terephthalic acid (TA) is used as the probe agent, which reacts rapidly with •OH to form 2-hydroxyterephthalic acid (HTA). HTA can be measured and quantified by using a fluorescence emission spectrometer (SHIMADZU, RF-6000A) at an excitation wavelength of 315 nm and an emission wavelength of 425 nm. Similarly, the concentration of $O_2^{\bullet-}$ is quantified by p-nitro-blue tetrazolium chloride (NBT) with a maximum absorption wavelength of 259 nm, which can be conveniently measured via a UV spectrophotometer (UV2600, Timemi). The concentration of $SO_4^{\bullet-}$ is estimated by quantitative assessment of the main degradation by−products from the reaction between $SO_4^{\bullet-}$ and the chemical probe

p-hydroxybenzoic acid (HBA) using high-performance liquid chromatography (HPLC). According to the stoichiometry of the reaction, 1 mol HBA can be reacted with 1 mol $SO_4^{\bullet-}$ to form hydroquinone, which was immediately converted to a stable byproduct, i.e., benzoquinone (BQ) by an excess of PMS[44]. In general, BQ is proportional to the concentration of $SO_4^{\bullet-}$. When an excess of HBA ($C_{HBA} > C_{BQ}$) is present, the generated BQ is relatively stable. To determine the concentration of $^1O_2$, furfuryl alcohol (FFA) was selected as a real-time "trap". When FFA was added to the Co-NC/PMS system, the concentration of FFA was measured and determined by HPLC, and then the concentration of $^1O_2$ was calculated based on the quantitative reaction relationship between FFA and $^1O_2$[45].

E. coli physical morphology and biochemical characterization

To study the K^+ ions leakage from bacterial cells during catalytic disinfection, the cell suspensions before and after treatment were collected and filtered through a microporous filter (pore size 0.45 μm). After filtration, the solution was acidified with 3 mol L^{-1} HNO_3, and the K^+ concentration was measured by a polarized Zeeman atomic absorption spectrophotometer (AAS) (Hitachi-2300, Japan). Intracellular DNA content: chromosomal DNA was extracted with Ezup column bacterial genomic DNA extraction kit (SK8255, Shanghai Shenggong), and then verified by DNA agarose gel electrophoresis (0.6% agarose gel, 100 V, 1XTAE buffer, 30 min). ATP detection kit (S0026, Biyuntian) was used to measure cell viability. The MDA concentration was calculated using a standard curve.

Staining of collected *E. coli* with dyes from the Live/Dead BacLight Bacterial Viability Kit (L7012, Molecular Probes, Inc., Eugene, OR) was observed by employing a confocal fluorescence microscope (Nikon ECLIPSE 80i, Japan)[46]. About 1 mL of bacterial solution (before and after filtration) was taken into a centrifuge tube. Then different dyes of 10 uL were added dropwise and incubated at 28 °C for 0.5 h with shaking evenly. And then, the samples were transferred to glass slides for observation. Among dyes, SYTO9 is a cell membrane-permeable nucleic acid dye capable of labeling all cells, no matter intact or damaged cell membranes. PI can only be transmitted to bacteria with damaged cell membranes. Thus, in a mixed bacterial population, bacteria with intact cell membranes appear in green (only stained by SYTO9), while the dead bacteria with damaged membranes appear in red (stained by SYTO9 and PI).

E. coli was firstly collected by centrifugation at 5000 rpm for 5 min, then 5 mL of glutaraldehyde (2.5%) was added and left overnight at 4 °C. Following that, it was washed twice with phosphate-buffered saline (PBS), then dehydrated in a sequential gradient of 30, 50, 70, and 90% ethanol for 10 min, respectively, and lastly twice with 100% ethanol for 20 min. The samples were then freeze-dried. Lastly, the collected samples were plated with gold, and their morphology changes were observed on a scanning electron microscope (JSM-7500F).

DATA AVAILABILITY

The data that support the findings of this study are available from the corresponding author upon reasonable request.

Received: 18 December 2022; Accepted: 26 May 2023;
Published online: 22 June 2023

REFERENCES

1. Mark, A. Science and technology for water purification in the coming decades. *Nature* **452**, 20 (2008).
2. Chopyk, J. et al. Comparative metagenomic analysis of microbial taxonomic and functional variations in untreated surface and reclaimed waters used in irrigation applications. *Water Res.* **169**, 115250 (2020).
3. Richter, A. P. et al. An environmentally benign antimicrobial nanoparticle based on a silver-infused lignin core. *Nat. Nanotechnol.* **10**, 817–823 (2015).
4. Duan, X. et al. Advanced oxidation processes for water disinfection: features, mechanisms and prospects. *Chem. Eng. J.* **409**, 128207 (2021).
5. Sedlak, D. L. & von Gunten, U. The chlorine dilemma. *Science* **331**, 42–43 (2011).
6. Wang, R. et al. Enhanced visible-light-driven photocatalytic sterilization of tungsten trioxide by surface-engineering oxygen vacancy and carbon matrix. *Chem. Eng. J.* **348**, 292–300 (2018).
7. Martínez, J. L. Antibiotics and antibiotic resistance genes in natural environments. *Science* **321**, 365–367 (2008).
8. Chen, Y., Ji, Q., Zhang, G., Liu, H. & Qu, J. Synergetic lipid extraction with oxidative damage amplifies cell-membrane-destructive stresses and enables rapid sterilization. *Angew. Chem. Int. Ed.* **133**, 7823–7830 (2021).
9. Xia, D. et al. Activation of persulfates by natural magnetic pyrrhotite for water disinfection: efficiency, mechanisms, and stability. *Water Res.* **112**, 236–247 (2017).
10. Klemes, M. J. et al. Polymerized molecular receptors as adsorbents to remove micropollutants from water. *Acc. Chem. Res.* **53**, 2314–2324 (2020).
11. López, A. et al. How does urban wastewater treatment affect the microbial quality of treated wastewater? *Pro. Saf. Environ.* **130**, 22–30 (2019).
12. Sharma, V. K., Zboril, R. & Varma, R. S. Ferrates: greener oxidants with multimodal action in water treatment technologies. *Acc. Chem. Res.* **48**, 182–191 (2015).
13. Moreira, F. C., Boaventura, R. A., Brillas, E. & Vilar, V. J. Electrochemical advanced oxidation processes: a review on their application to synthetic and real wastewaters. *Appl. Catal. B. Environ.* **202**, 217–261 (2017).
14. Guo, Z. et al. Single-atom Mn–N4 site-catalyzed peroxone reaction for the efficient production of hydroxyl radicals in an acidic solution. *J. Am. Chem. Soc.* **141**, 12005–12010 (2019).
15. Duan, X., Sun, H. & Wang, S. Metal-free carbocatalysis in advanced oxidation reactions. *Acc. Chem. Res.* **51**, 678–687 (2018).
16. Giannakis, S. A review of the concepts, recent advances and niche applications of the (photo) Fenton process, beyond water/wastewater treatment: surface functionalization, biomass treatment, combatting cancer and other medical uses. *Appl. Catal. B. Environ.* **248**, 309–319 (2019).
17. Lee, J., Von Gunten, U. & Kim, J.-H. Persulfate-based advanced oxidation: critical assessment of opportunities and roadblocks. *Environ. Sci. Technol.* **54**, 3064–3081 (2020).
18. Ren, W. et al. The intrinsic nature of persulfate activation and N-doping in carbocatalysis. *Environ. Sci. Technol.* **54**, 6438–6447 (2020).
19. Meng, C. et al. Angstrom-confined catalytic water purification within Co-TiO_x laminar membrane nanochannels. *Nat. Commun.* **13**, 1–10 (2022).
20. Oh, W.-D., Dong, Z. & Lim, T.-T. Generation of sulfate radical through heterogeneous catalysis for organic contaminants removal: current development, challenges and prospects. *Appl. Catal. B. Environ.* **194**, 169–201 (2016).
21. Li, J. et al. Understanding of the oxidation behavior of benzyl alcohol by peroxymonosulfate via carbon nanotubes activation. *ACS Catal.* **10**, 3516–3525 (2020).
22. Hodges, B. C., Cates, E. L. & Kim, J.-H. Challenges and prospects of advanced oxidation water treatment processes using catalytic nanomaterials. *Nat. Nanotechnol.* **13**, 642–650 (2018).
23. Lim, J., Yang, Y. & Hoffmann, M. R. Activation of peroxymonosulfate by oxygen vacancies-enriched cobalt-doped black TiO_2 nanotubes for the removal of organic pollutants. *Environ. Sci. Technol.* **53**, 6972–6980 (2019).
24. Yin, Y. et al. Boosting Fenton-like reactions via single atom Fe catalysis. *Environ. Sci. Technol.* **53**, 11391–11400 (2019).
25. Yang, Y. et al. Sustainable redox processes induced by peroxymonosulfate and metal doping on amorphous manganese dioxide for nonradical degradation of water contaminants. *Appl. Catal. B. Environ.* **286**, 119903 (2021).
26. Zhang, Y.-J. et al. Simultaneous nanocatalytic surface activation of pollutants and oxidants for highly efficient water decontamination. *Nat. Commun.* **13**, 1–13 (2022).
27. Wu, X. et al. Single-atom cobalt incorporated in a 2D graphene oxide membrane for catalytic pollutant degradation. *Environ. Sci. Technol.* **56**, 1341–1351 (2021).
28. Wang, Z. et al. Cobalt single atoms anchored on oxygen-doped tubular carbon nitride for efficient peroxymonosulfate activation: simultaneous coordination structure and morphology modulation. *Angew. Chem. Int. Ed.* **61**, e202202338 (2022).
29. Mady, A. H., Baynosa, M. L., Tuma, D. & Shim, J.-J. Heterogeneous activation of peroxymonosulfate by a novel magnetic 3D γ-MnO_2@ $ZnFe_2O_4$/rGO nanohybrid as a robust catalyst for phenol degradation. *Appl. Catal. B. Environ.* **244**, 946–956 (2019).
30. Kang, J. et al. Degradation of cosmetic microplastics via functionalized carbon nanosprings. *Matter* **1**, 745–758 (2019).

31. Wu, R. et al. Magnesium-functionalized ferro metal–carbon nanocomposite (Mg-FeMeC) for efficient uranium extraction from natural seawater. *ACS EST Water* **1**, 980–990 (2021).
32. Li, X. et al. Single cobalt atoms anchored on porous N-doped graphene with dual reaction sites for efficient Fenton-like catalysis. *J. Am. Chem. Soc.* **140**, 12469–12475 (2018).
33. Huang, H. et al. Photothermal-assisted triphase photocatalysis over a multifunctional bilayer paper. *Angew. Chem. Int. Ed.* **60**, 22963–22969 (2021).
34. Dou, J. et al. Biochar co-doped with nitrogen and boron switching the free radical based peroxydisulfate activation into the electron-transfer dominated nonradical process. *Appl. Catal. B Environ.* **301**, 120832 (2022).
35. Zhu, J. et al. Degradation of phosphonates in Co (II)/peroxymonosulfate process: performance and mechanism. *Water Res.* **202**, 117397 (2021).
36. Huang, Z. et al. The consortium of heterogeneous cobalt phthalocyanine catalyst and bicarbonate ion as a novel platform for contaminants elimination based on peroxymonosulfate activation. *J. Hazard. Mater.* **301**, 214–221 (2016).
37. Zhang, R. et al. The photothermal synergy effect of pure $Ti_3C_2T_x$ in antibacterial reaction and its mechanism. *Environ. Sci: Nano* **8**, 1446–1455 (2021).
38. Yang, Z., Qian, J., Yu, A. & Pan, B. Singlet oxygen mediated iron-based Fenton-like catalysis under nanoconfinement. *Proc. Natl Acad. Sci. USA* **116**, 6659–6664 (2019).
39. Bao, Y. et al. Generating high-valent iron-oxo≡ Fe^{IV}= O complexes in neutral microenvironments through peroxymonosulfate activation by Zn-Fe layered double hydroxides. *Angew. Chem. Int. Ed.* **61**, e202209542 (2022).
40. Zong, Y. et al. Unraveling the overlooked involvement of high-valent cobalt-oxo species generated from the cobalt (II)-activated peroxymonosulfate process. *Environ. Sci. Technol.* **54**, 16231–16239 (2020).
41. Huang, M. et al. Facilely tuning the intrinsic catalytic sites of the spinel oxide for peroxymonosulfate activation: from fundamental investigation to pilot-scale demonstration. *Proc. Natl Acad. Sci. USA* **119**, e2202682119 (2022).
42. Zhen, Y. et al. Selectively efficient removal of micropollutants by N-doped carbon modified catalytic ceramic membrane: synergy of membrane confinement and surface reaction. *Appl. Catal. B. Environ.* **324**, 122188 (2023).
43. Wang, Z. et al. Cobalt single atoms anchored on oxygen-doped tubular carbon nitride for efficient peroxymonosulfate activation: simultaneous coordination structure and morphology modulation. *Angew. Chem. Int. Ed.* **134**, e202202338 (2022).
44. Oh, W.-D., Dong, Z., Ronn, G. & Lim, T.-T. Surface–active bismuth ferrite as superior peroxymonosulfate activator for aqueous sulfamethoxazole removal: performance, mechanism and quantification of sulfate radical. *J. Hazard. Mater.* **325**, 71–81 (2017).
45. Huang, R. et al. Insights into the pollutant electron property inducing the transformation of peroxymonosulfate activation mechanisms on manganese dioxide. *Appl. Catal. B. Environ.* **317**, 121753 (2022).
46. Zhang, R. et al. Sterilization of *Escherichia coli* by photothermal synergy of WO_{3-x}/C nanosheet under infrared light irradiation. *Appl. Catal. B. Environ.* **54**, 3691–3701 (2020).

ACKNOWLEDGEMENTS

This work is supported by the National Natural Science Foundation of China (Nos. 51872147 and 22136003), the Hubei Provincial Natural Science Foundation of China (No. 2022CFA065), and the 111 Project (D20015).

AUTHOR CONTRIBUTIONS

C.L.: Investigation, interpretation of the data, validation, writing, and revision. J.L. and Q.X.: Investigation and formal analysis. X.Y.K., Y.H., and P.K.W.: Formal analysis and conceptualization. N.H. and L.Y.: Conceptualization, methodology, supervision, funding acquisition, and writing.

COMPETING INTERESTS

The authors declare no competing interests.

ADDITIONAL INFORMATION

Supplementary information The online version contains supplementary material available at https://doi.org/10.1038/s41545-023-00259-5.

Correspondence and requests for materials should be addressed to Niu Huang or Liqun Ye.

Reprints and permission information is available at http://www.nature.com/reprints

Publisher's note Springer Nature remains neutral with regard to jurisdictional claims in published maps and institutional affiliations.